The Potential of SiC Cascode JFETs in Electric Vehicle Traction Inverters

Ruizhu Wu, Jose Ortiz Gonzalez, *Member, IEEE*, Zarina Davletzhanova, Philip Mawby, *Senior Member, IEEE*, Olayiwola Alatise, *Member, IEEE*

Abstract

The benefits of implementing SiC devices in EV powertrains has been widely reported in various studies. New generations of SiC devices including planar MOSFETs, trench MOSFETs and more recently, cascode JFETs have been released by various manufacturers. SiC cascode devices comprise of low voltage silicon MOSFETs for gate driving and high voltage depletion mode SiC JFETs for voltage blocking. These devices are particularly interesting because it avoids the known reliability issues of SiC gate oxide traps resulting in threshold voltage drift. In this paper, an EV powertrain is simulated using experimental measurements of conduction and switching energies of various SiC devices including 650V trench, 900V planar and 650V cascode JFETs. Unlike previous papers where losses are calculated using models based on datasheet parameters, here static and dynamic measurements on the power devices at different currents and temperatures are used to calculate losses over simulated driving cycles. Field-stop IGBTs are also evaluated. The 3-phase 2-level inverter model is electrothermal by accounting for the measured temperature dependence of the losses and uses accurate thermal networks derived from datasheets. Converter efficiency and thermal performance are compared for each device technology. Results show that SiC cascode JFETs have great potential in EV powertrain applications.

I. Introduction

Silicon carbide (SiC) is well known to have improved energy conversion efficiency in EVs compared to comparatively rated silicon devices [1]. The implementation of SiC power devices in EV powertrains has been widely investigated by various researchers. Before SiC MOSFETs became widely available, the prospects of SiC JFET/SiC SBD in EV traction inverters was investigated and the results showed better thermal performance due to lower losses compared to silicon IGBT based converters [2-4]. However, as SiC MOSFETs became widely available, attention was switched to MOSFETs due to the preferred normally OFF operation and easier gate driving system [5]. To this end, high power SiC MOSFET based traction inverters have been demonstrated by various researchers. In [6], a 220 kW low inductance power module was implemented in 1.2 kV SiC trench MOSFETs (with 25mm^2 chip size for 100 A_{RMS} current) on an 800V DC bus EV drivetrain. An output power density of 57kW/L was achieved which was 57% higher than an IGBT power module with the same rating. The switching frequency ranged from 16 kHz to 24 kHz. In [7], a 100kW SiC MOSFET based traction inverter with a power density of 34kW/L was demonstrated operating on a 400V DC bus with a switching frequency of 40kHz. In [8], a power device technology case study was performed on the powertrain of a 2016 BMW i3 comprising of a 125 kW powertrain running of a 360 V DC bus with a 3-phase 2-level VSC running at 5 kHz switching frequency. The performance of 650 V IGBTs from Infineon in the drivetrain was compared to a (i) 650V 22mΩ SiC power MOSFET (ii) 650V 30mΩ SiC power MOSFET and a (iii) 900V 10mΩ SiC power MOSFET. The power losses in the devices were calculated from datasheets and used as inputs to the model however, the model was not fully electrothermal and did not quantify the thermal stresses across the devices.

In [9], the energy conversion performance of a 40 kW 3-phase, 2-level VSC switching at 5kHz was evaluated for different power device technologies namely, silicon IGBTs/PiN diode, SiC JFET/SiC SBD, SiC MOSFETs/SiC SBD and a SiC BJT/SiC SBD. In the study, all the devices were rated at 1.2kV with current ratings approximately around 20A at 25°C. The conduction and switching losses were calculated using formula's in combination with parameters taken from datasheets. The results from this paper showed that the SiC BJT were predicted to have the lowest losses, followed by the SiC MOSFET, SiC JFET and then the silicon IGBT. The model however was not an electrothermal model in that it did not account for the temperature dependency of the device losses and did not yield the average junction temperature and temperature swing across the device. In [10], 1.2 kV and 650 V Silicon IGBT and SiC MOSFET modules were characterised experimentally and the measured losses were mapped into a 450V 2-level and 900V 3-level NPC converter both with power ratings of 60kW and a switching frequency of 12 kHz. The simulations were static in that a driving cycle was not simulated and the power losses were calculated assuming a modulation index of 0.9. The results showed an approximate 35% reduction in power loss in the SiC MOSFET module compared to the silicon IGBT module. In [11, 12], 1.2kV SiC MOSFET and silicon IGBT power modules were simulated in an EV drivetrain with an 600V DC link voltage switching at 8kHz switching frequency. In this paper, the power losses were calculated using standard formulae for a PWM switched inverter and the junction temperature is

This work was supported by the UK Engineering and Physical Science Research Council (EPSRC) through the grant reference EP/R004366/1 and reference EP/R004927/1.

All the authors are with the School of Engineering, University of Warwick, CV4 7AL, Coventry, UK. (email: robert.wu.1@warwick.ac.uk, j.a.ortiz-gonzalez@warwick.ac.uk, zarina.davletzhan@gmail.com, P.A.Mawby@warwick.ac.uk, o.alatise@warwick.ac.uk,)

calculated using transient thermal impedance matrices. In [13], a SiC MOSFET module comprised of 1.2 kV SiC trench MOSFETs and SBDs, a 1.2kV Silicon IGBT module with silicon diodes and a hybrid module with Si IGBTs and SiC SBDs are all compared in an EV drivetrain with a 20kWh driving cycle. The results showed significant reduction in total losses with the SiC hybrid and full SiC modules showing up to 45% and 80% reduction in total losses compared to the IGBT module at low vehicle speeds. However, as the vehicle speed is increased, the poor conduction performance in the SiC devices at high currents means the efficiency improvement is lost. In [14], a 30kW SiC MOSFET based EV traction inverter was demonstrated with 3 times lower peak power loss and 2 times higher the power density compared to a silicon IGBT based inverter. The switching frequency of the SiC based inverter was twice that of the IGBT based inverter. In [15], SiC MOSFET based inverters were demonstrated to have better efficiency and lower output voltage distortion compared silicon IGBT inverters due to higher switching speed and smaller output capacitance.

Most of the papers discussed above have focussed on SiC MOSFETs. However, the more recently released SiC cascode device offers new opportunities for EV powertrains. SiC power MOSFETs are known to be susceptible to threshold voltage drift from bias temperature instability (BTI) [16-18]. This is due to the charging and discharging to traps in the SiC/SiO_2 interface. Thermal oxidation of SiC results in significantly more interface trap density than thermal oxidation of silicon, hence, BTI is more evident in SiC. However, SiC cascode devices combine a low voltage (LV) silicon MOSFET at the input with a high voltage SiC JFET at the output, hence, the reliability issues regarding the SiC gate oxide are completely avoided. A schematic of the SiC Cascode JFET is shown in Fig. 1 where the drain of the low side silicon MOSFET is connected to the source of the normally ON SiC JFET. Since the gate of the normally ON-JFET is connected to the source of the LV silicon MOSFET, the JFET behaves in enhancement mode (with positive threshold voltage) if the breakdown voltage of the LV silicon MOSFET is greater than the magnitude of the threshold voltage of the SiC JFET [19, 20].

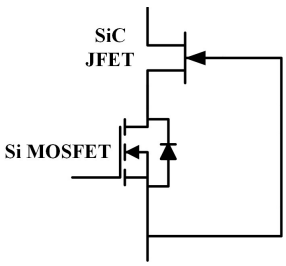

Fig. 1. Schematic of SiC cascode JFET

Here, the potential performance of the SiC cascode JFET in an EV drivetrain has been investigated alongside comparatively rated SiC planar MOSFETs, SiC trench MOSFETs and a silicon IGBT. In this paper, static and dynamic measurements have been used as inputs into a 300kW EV drivetrain model with a permanent magnet motor and a system coolant temperature of 60°C. Since the losses have been characterised at different currents and temperatures, the model is fully electrothermal since look-up tables have been used to relate the losses to the device junction temperature. Thermal networks specific to each device have been developed from transient thermal impedance characteristics. Section II presents the static and dynamic measurements of the devices. Section III introduces the fully coupled electrothermal model and the power loss calculations.

II. Static and Dynamic Measurements on Power Devices

The ON-state losses have been characterised using the circuit in Fig. 2 (a) while the switching losses were characterised using a double pulse test set-up shown in Fig. 2 (b). The devices under consideration are the 650V SiC trench MOSFET from ROHM (SCT3060AL), the 900V SiC planar MOSFET from Wolfspeed (C3M0065090D), the SiC cascode device from United SiC (UJ3C065080K3S) and a silicon IGBT from ROHM (RGT40TS65D). Using the manufacturer datasheets as a reference, the selected devices are of similar current ratings (between 31A and 40A at 25°C and between 20A and 27A at 100°C). The number of devices needed to implement each switch of the converter at a defined system cooling temperature, rated current and current power density will be discussed in section III. The turn-ON and turn-OFF losses of both the transistor and the diode were measured at different junction temperatures (25°C, 75°C and 150°C) and load currents (10 A and 20 A).

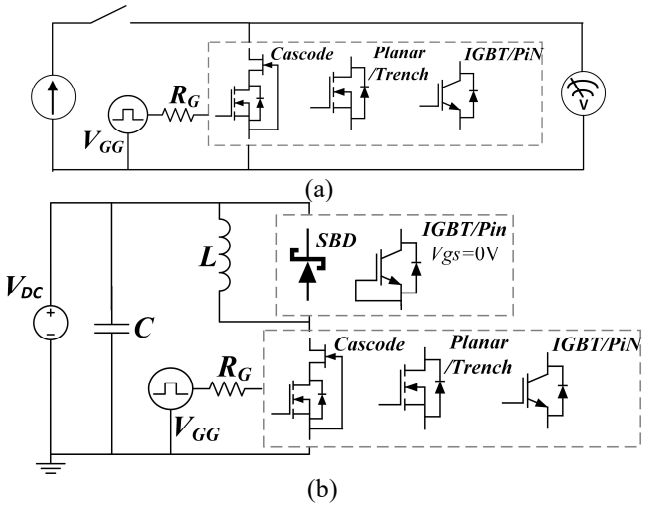

Fig. 2. Test rig for (a) ON-state loss and (b) Switching loss.

The switching energy as well as the current and voltage commutation rates have been measured for all the technologies. Fig. 3 shows the current turn-ON of the power devices where the SiC cascode outperforms all other technologies in terms of the *dI/dt*. Fig. 4 shows the measured *dI/dt* for all the technologies for a range of gate resistances from 10Ω to 100Ω. The SiC cascode device exhibits the highest turn-ON *dI/dt* followed by the planar device, the silicon IGBT and the SiC trench MOSFET. The trend is similar for the turn-OFF *dV/dt* as shown in Fig. 5. The measured switching energies at different gate resistances are shown in Fig. 6(a) where the SiC cascode device is the best

performing, followed by the SiC planar, SiC trench (at lower R_G) and the silicon IGBT. At smaller gate resistances (33Ω and below), the SiC trench outperforms the IGBT however at higher gate resistances (68Ω and 100Ω) the IGBT performs better. The results in Fig. 6(b) show the switching energy at different temperatures with R_G=33Ω where the order of performance is the SiC cascode, SiC planar, SiC trench and then the Si IGBT.

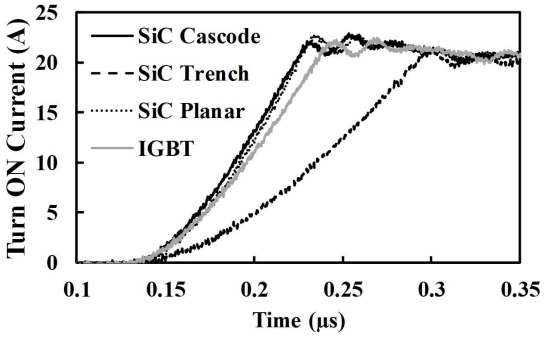

Fig. 3. Turn-ON current transient for the different technologies with 400 V at 25°C

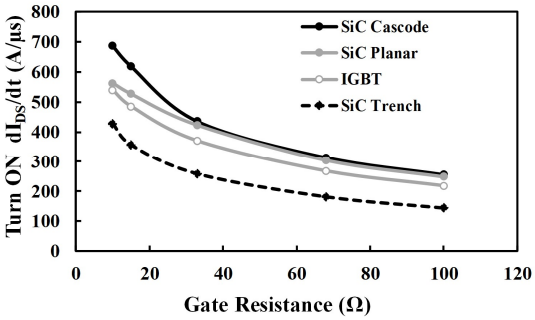

Fig. 4. Turn-ON *dI/dt* for the different technologies with 400 V at 25°C

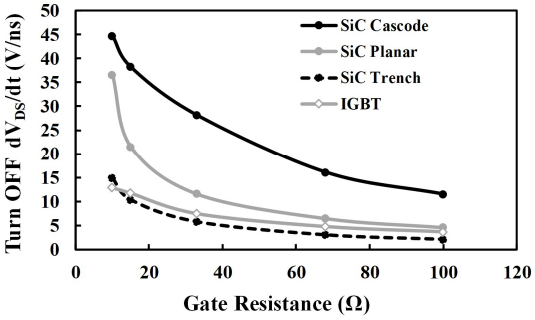

Fig. 5. Turn-OFF *dV/dt* for the different technologies with 400 V at 25°C

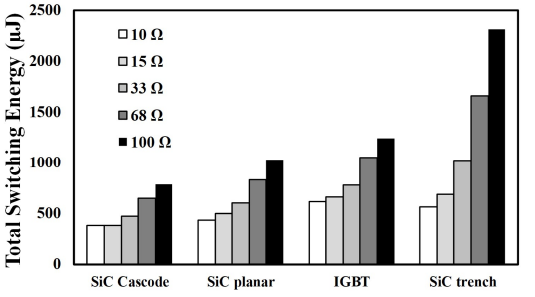

(a)

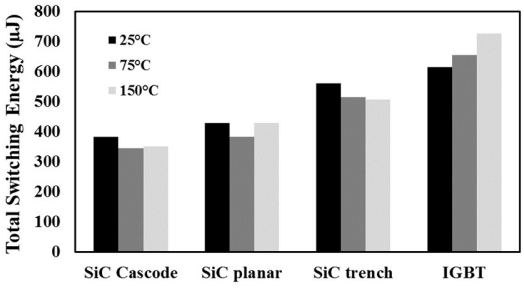

(b)

Fig. 6. Total switching energy on all technologies at (a) different switching rates and (b) junction temperatures.

The choice of diode used is very critical since the reverse recovery current of the diode contributes to transistor turn-ON losses. In the previous measurements, the same high side 650V SiC SBD from Wolfspeed (with datasheet reference C3D10065) was used for all transistors. Fig. 7 shows the measured total switching energy for the IGBT switched with a SiC SBD and the IGBT switched with a PiN diode. The PiN diode used was the IGBT co-packaged PiN diode. The measurements have been performed at 25°C, 75°C and 150°C. The results show significant additional losses in the IGBT switched with the PiN diode because of the additional reverse recovery current from the high side PiN diode. The losses also increase with temperature since the reverse recovery charge increases with temperature due to the positive temperature coefficient of carrier lifetime.

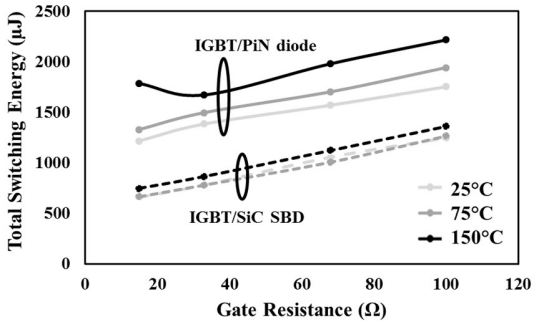

Fig. 7. Total switching losses of IGBTs switched with PiN and Schottky diodes at different temperatures

The ON-state losses were measured by passing a DC current of 20 A through the device and measuring the ON-state voltage drop over a period of 3 seconds. The specific ON-state resistance for the different technologies is shown in Fig. 8. The results show that the SiC cascode device is the best performing device, followed by the planar MOSFET, the trench MOSFET and then the silicon IGBT. Since, the duration of the current pulse in Fig. 8 is long enough for self-heating to raise the junction temperature, the results in Fig. 8 also shows that the conduction losses of the SiC trench MOSFET is temperature invariant since the ON-state voltage remains constant over the 3 second heating pulse. In the other devices, there is an increase in the ON-state

resistance with time due to the positive temperature coefficient of the ON-state resistance.

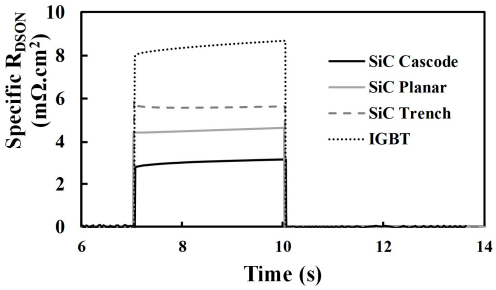

Fig. 8. Specific ON-state resistance of the different technologies

III. EV DRIVETRAIN MODELLING

A. *Converter Rating:*

In this paper, a 300 kW, 3-phase, 2-level, voltage source inverter is simulated in an EV drivetrain. The DC link voltage in the simulation is 400V, the peak current in each phase of the converter is 800 A (an additional 15% headroom will be left) and the coolant temperature of the inverter is assumed to be 60°C. Typically, some manufacturers implement the inverter as power modules with parallel devices on custom designed direct bonded copper (DBC) substrates while others have more recently implemented the inverter as discrete devices in custom designed thermally conducting and electrically isolated packages. In both cases, several power devices are required for sharing current with the devices designed to operate at a defined current density. In the analysis here, we assume the devices share current equally, hence, the conduction losses are specific to the operating current density and the switching losses depend on the number of parallel devices. By measuring the conduction and switching losses of a single device, we can therefore extrapolate to the switching unit. Before determining how many devices are required for conducting the peak phase current, it is interesting to note that the respective manufacturers, according to their datasheets, recommend their devices are driven at different current densities (which has been calculated by dividing the rated current by the chip area deduced from decapsulated devices). The current densities for each device technology evaluated in section II are shown in Table I where the SiC cascode JFET operates at the highest current density (9.35 A/mm^2) followed by the SiC planar MOSFET, the SiC trench MOSFET and lastly, the silicon IGBT. The SiC cascode JFET operates at almost twice the current density of the SiC planar and trench MOSFETs.

The goal of the measurement/simulation study is to compare the latest generation of power device technologies. To make the comparison a fair one, two scenarios have been considered regarding the number of parallel devices required for converter operation, namely (i) identical rated current for all devices and (ii) identical current density for all devices. In the first scenario, the number of devices required to conduct the peak phase current is calculated by dividing the peak phase current by the device rated current at a case temperature of 60°C. The current rating at 60°C case temperature is determined by linear interpolation between the rated currents specified at a case temperature of 25°C and a case temperature of 100°C. Under this condition, the device is operated at the recommended current density and the current rating of each device is used to size the converter. The numbers are derived as shown in Table I. The second scenario is based on comparing all technologies at the same current density (meaning that the total area of the semiconductor chip is identical in all test cases). The reference current density is chosen as 3.16 A/mm^2, which is the recommended current density for the silicon IGBT used in this study. The numbers derived are also shown in Table I, where it is clear to see that the SiC Cascode JFET requires the highest number of devices because it operates at a much higher current density compared to the other technologies (because it has the smallest chip area). The silicon IGBT requires the least devices because it operates at the lowest current density (i.e. it has the largest chip area). The numbers of diodes are considered to be the same as the transistors.

Table I

Device Data

	Cascode SiC JFET	SiC Planar	SiC Trench	Si IGBT
Datasheet reference	UJ3C065 080K3S	C3M006 5090D	SCT3060 AL	RGT40T S65D
Voltage rating (V)	650	900	650	650
On-resistance at 25 °C (mΩ)	80 (V_{GS}=12)	65 (V_{GS}=15)	60 (V_{GS}=18)	n/a
Current rating at T_{case} = 25°C (A)	31	36	39	40
Current rating at T_{case} = 60 °C (A)	27.3	29.9	33.4	30.7
Current rating at T_{case} = 100°C (A)	23	23	27	20
Chip size (mm^2)	2.92	6.05	7.76	9.71
Rated current density (A/mm^2)	9.35	4.94	4.30	3.16
No. of chips for same current rating - 900A	33	30	27	30
No. of chips for same current density – 3.16 A/mm^2	100	48	38	30
Junction-case Thermal Resistance (K/W)	0.79	1.0	0.91	1.04

Operating the SiC devices at high current densities will reduce cost since less devices are required however, this may have adverse consequences on reliability since the average junction temperature of each chip is much higher. On the other hand, reducing the current density has obvious reliability advantages (lower junction temperatures) but this comes with significant additional cost.

B. *EV Powertrain Model*

The simulation model is fully implemented in Matlab/Simulink including the powertrain model and the electrothermal power loss calculator which takes into account devices' thermal response as shown in Fig. 9. The traction inverter is a 3-phase 2-level converter which controls a 4-pole permanent magnet synchronous motor (PMSM). The parameters of the PMSM are dynamically acquired from a dynamic motor model. The stator current i_{stator} and the electric angle of the PMSM rotor θ_{rotor} are measured for controlling the traction

inverter. PMSMs are the most widely used type of motor in electric vehicle powertrains due to its superior performance at low ratings compared to induction motors. In this study, a 300 kW PMSM with experimentally measured motor parameters is used in the EV powertrain model. If the dynamic parameters (stator inductance, stator resistance and flux linkage) are unknown, then the parameters of the motor can be set as constants while the i_d and i_q references are generated using the maximum torque per ampere (MTPA) control for low speed and field weakening (FW) control for high speed. MTPA control minimizes stator current at a certain torque in machines producing both PM and reluctance torques, and FW control weakens the stator flux linkage by controlling d-axis current when the voltage limit is reached. Once the i_d and i_q reference currents are generated by either MTPA or FW control, they are fed into the current controller which controls machine stator currents and generates the PWM signals of the traction inverter [21].

However, in this paper, the torque controller has been replaced with LUTs of stator current values that have been measured experimentally. Fig. 9 shows the EV motor control system including the current controller, LUTs, inverter, PMSM etc. These LUTs contain i_d and i_q values for different torque and speed conditions. The parameters of the PMSM are not constant but dynamic at different operating points: the flux linkage λ varies with the q-axis stator current i_q; the phase resistance R_s varies with the motor speed v_{motor} (due to the skin effect where AC resistance of the stator coils increases with frequency); the inductances in quadrature and direct axis (q and d-axis), L_d and L_q vary with the d and q-axis stator current i_d and i_q. For the current controller, the conventional proportional-integral (PI) control is used and the gains are selected using internal model control (IMC) which simplifies the parameter design [22, 23]. It should be noted that the control gains are related to R_s, L_d and L_q that change with operating points. Therefore, the control gains must also be updated dynamically as shown in the dashed blue box in Fig. 9.

C. *Electrothermal Model for Power Loss Calculations*

The power loss in the traction inverter consists of transistors' conduction loss, turn-ON and OFF losses as well as the anti-parallel diodes' conduction loss and reverse recovery loss. The measurements presented in section II are used to build LUTs. Unlike previous EV traction inverter simulations that use mathematical models based on datasheet parameters [11, 13, 24], the EV simulation in this paper uses measured switching energies and calculates power losses at each simulation step. The transistor and diode losses depend on current and temperature, hence, measurements have been performed on all the device technologies at different currents (10A and 20A) and different temperatures (25°C, 75°C and 150°C). LUTs are built for the conduction and switching losses for the transistor and the diodes.

Fig. 10 shows the loss calculator for the transistor's conduction and turn-on losses in the simulation. Fig. 10 (a) shows the process for calculating the transistor's conduction loss. The positive component (the component flowing through the transistor) is first extracted by multiplying the current by the output of the logic operation which indicates if the device is ON or OFF. Then the positive current $i(>0)$ and junction temperature T_j are fed into the 2-D LUT to get the voltage across the device, v in the conducting state. The LUT comprises of the datasheets offered voltage drop (verified by experiments) and its temperature dependency. The last step is to find the product between v and $i(>0)$ to get the conduction loss. When calculating the diode's conduction loss, replacing the '>0' logic operating with '<0' to extract the current flowing through the diode and adding an absolute mathematic operation before the LUT to get the absolute value of the current.

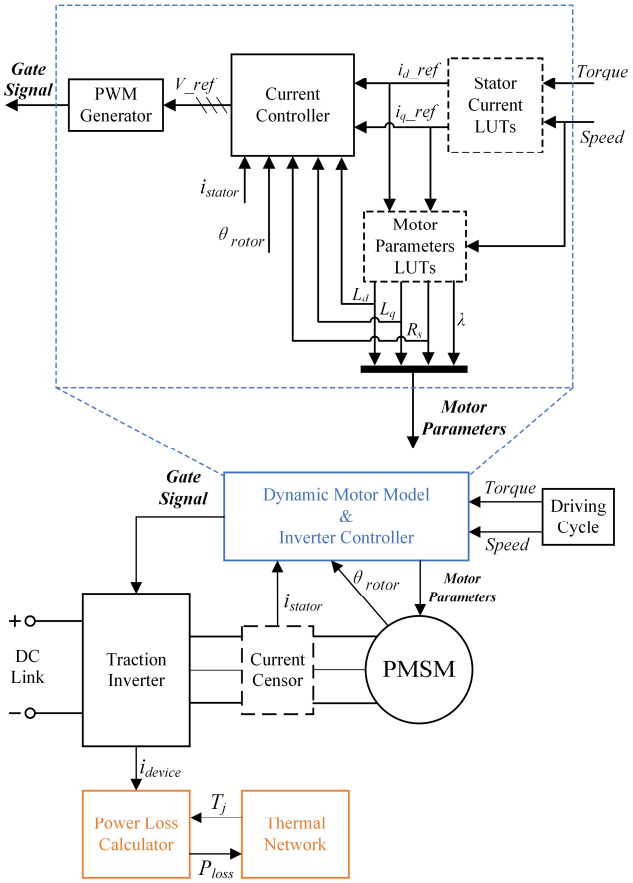

Fig. 9. Whole simulation model including the powertrain model and the electrothermal power loss calculator

Fig. 10 (b) shows the process for calculating the transistor's turn-on loss. The input into the algorithm is the PWM sinusoidal current which is determined by the power demand of the motor. The algorithm uses the polarity of the current to determine whether the transistor is conducting (if $i > 0$) or if the diode is conducting ($i < 0$). An edge detector logic block is used against the gate voltage signal to determine the turn-ON instant. The output of the edge detector, which is a binary '1' or '0', is multiplied by the positive current and fed into the LUT to determine the corresponding switching energy (E_{on}) at the defined temperature. The LUT comprises of the measured turn-ON and turn-OFF switching energies (at different currents and temperatures) presented in section II of the paper. Note that the pulse duration of the sampled positive current (i_{samp}) is equal to the minimum simulation step size (T_s) which is 2µs. The

switching energy is divided by 2μs to determine the average power loss. In reality, this switching energy is dissipated over the transient duration of the switching device (which can be as low as 10ns depending on the parasitic capacitances and gate resistances). However, due to limited computational resource, it can be assumed that this switching energy is dissipated over 2μs without loss of accuracy since the thermal time constant is much larger than 2μs. When calculating turn-OFF loss, making the edge detector detect the turn-OFF instant.

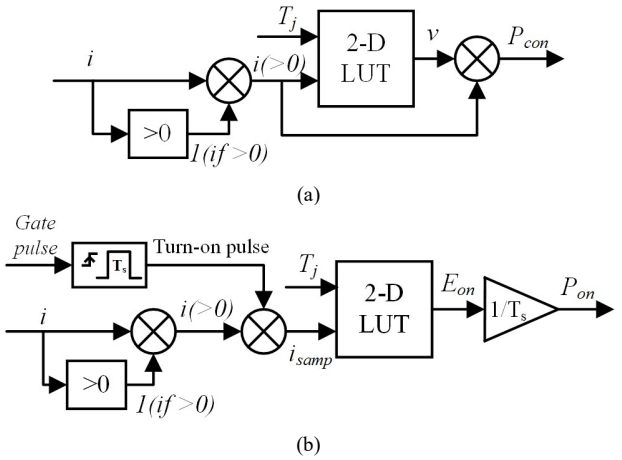

Fig. 10. Loss calculator diagrams: (a) transistor conduction loss; (b) transistor turn-on loss.

Fig. 11 shows the simulated load current (positive half cycle), gate signal, conduction and switching loss profiles using the algorithms described in Fig. 10. During the positive half cycle of the load current, current only flows through the transistor at the top arm. The transistor conduction loss is only calculated when the transistor is conducting current as intended while the turn-on loss is only calculated at each turn-on instant.

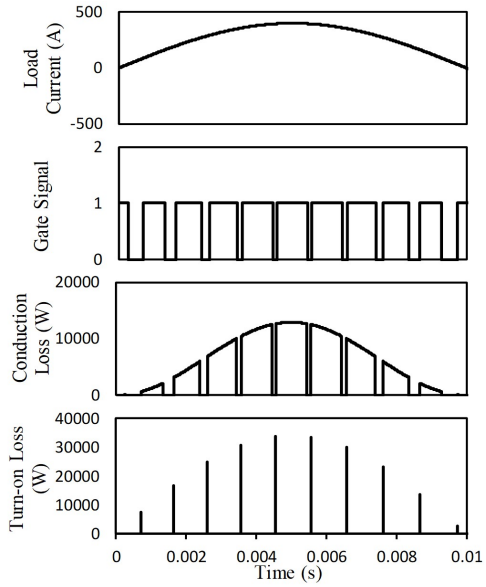

Fig. 11. Conceptual plots for loss calculation process: from top to bot are load current, gate signal of one device, conduction loss of the transistor and turn-on loss of the transistor.

The sum of all the three transistor losses (conduction, turn-ON and OFF) is fed into the thermal network (Forster or Cauer) to yield an instantaneous junction temperature (T_j) to maintain the temperature dependency of the power dissipation. The thermal networks are derived from the transient thermal impedance characteristics given on device manufacturer datasheets. Since the devices have different thermal impedances and different loss performance, they will exhibit different temperature excursions under identical loading conditions. The case temperature of the thermal network is held at 60°C. A similar process is done for the diode, the switching power algorithm is activated if a negative current is detected. A similar LUT of temperature and current dependent switching energy is used to determine the diode switching losses and its contribution to the junction temperature. Then, the total diode loss is fed into the diode's thermal network to obtain the diode junction temperature.

IV. EV Modelling Results

The results of the EV simulations in section III coupled with the experimental measurements in section II are presented in this section. Five device technology combinations have been simulated namely (i) SiC Cascode JFET with SiC SBD (ii) SiC planar MOSFET with SiC SBD (iii) SiC trench MOSFET with SiC SBD (iv) silicon IGBT with SiC SBD and (v) silicon IGBT with PiN diode. Refer to table I for the datasheet references. Here, two different driving cycle cases are evaluated since the operating point of the EV will stress the converter in different ways. The operating conditions, power losses and junction temperatures are shown for each case. Case 1 is a low torque and average speed profile including acceleration and deceleration. Case 2 shows the profile of a full power acceleration process (peak current is applied constantly). In Case 1 and 2, the numbers of parallel devices in each arm are selected according to the rated values in datasheets meaning the devices operate at different current densities and are therefore subject to different levels of electrical stress. In other words, the total semiconductor area for each device technology is different.

To study device performances at the same electrical stress level (the same current density), the numbers of parallel devices is selected to maintain the same active area (and current density). The EV simulation is run with the different SiC devices operating at the current density of the IGBT chip (3.16 A/mm^2). This is done in Case 3. The device numbers are listed in Table I.

A locked rotor condition is simulated in Case 4 to investigate the critical temperature of each technology. The locked rotor test is considered as the 'worst' case because that the converter is stressed by the peak current with very low fundamental frequency which consequently results in the largest swings of device junction temperature.

A. Case 1 – low torque average speed

For Case 1, the speed and torque profiles in the time period between 22 and 42 s of Worldwide Harmonized Light Vehicle Test Procedure (WLTP) are used. During this period, the vehicle is running at the speed around 40 km/h with low torque power. An acceleration and a deceleration process are included. During

the deceleration period, negative torque is applied thus the power flows back from the motor to the DC link. This is also known as regenerative braking and the current is mostly flowing through the diode in this process.

Fig. 12 shows the power loss under the defined driving cycle conditions. The results show that SiC devices have lower power losses than Si IGBT with the Cascode/SBD demonstrating the lowest power loss followed by Planar/SBD, Trench/SBD, IGBT/SBD and IGBT/PiN. SiC devices have significantly lower switching loss as expected due to their faster switching capability. In terms of conduction loss, SiC devices still show great advantage because they have lower on-resistance than Si devices at low current which is the operating condition in this case, i.e. motor is running at low torque which results in low current in the traction inverter.

The vehicle speed, motor torque, stator current and active/reactive power at the stator side in this case are shown in Fig. 13. Fig. 14 shows the simulated junction temperatures of the five groups in this case. From top to bottom are the Cascode/SBD, Planar/SBD, Trench/SBD, IGBT/SBD and IGBT/PiN. Overall SiC devices have lower average temperature with smaller swings. Planar and trench devices perform the best and the cascode follows tightly with slightly bigger fluctuation. Junction temperature is directly related to the power loss in the chip and the results correlate to the power loss performance.

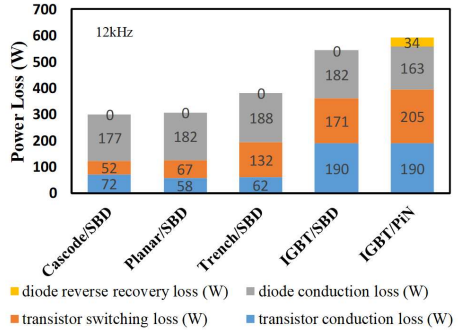

Fig. 12. Average power loss during WLTP cycle 22-42s.

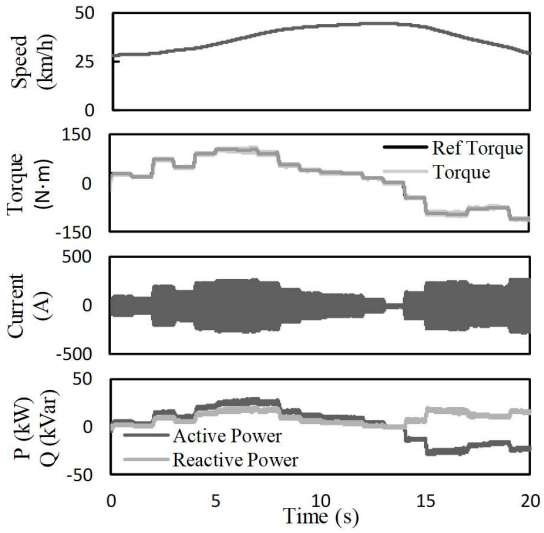

Fig. 13. Operating conditions during WLTP cycle 22-42s, from top to bottom are: vehicle speed, motor torque, stator current, electric active and reactive power of the motor.

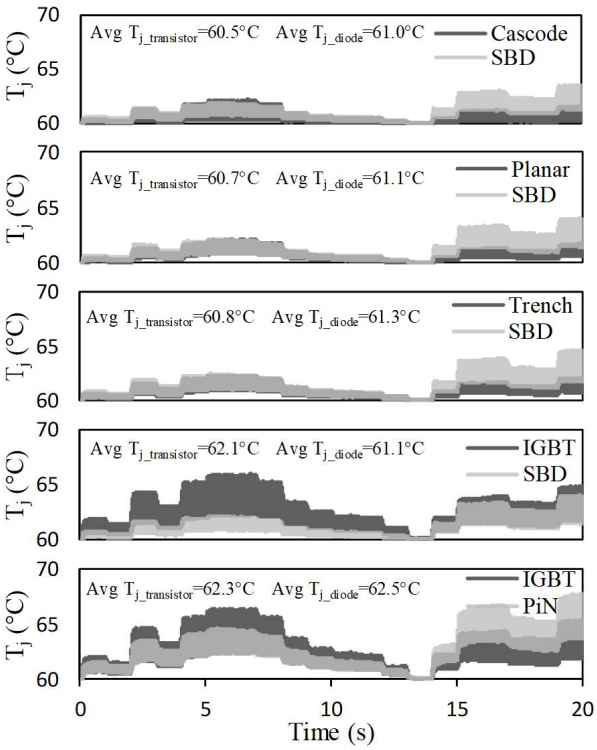

Fig. 14. Junction Temperatures, from top to bottom are: Cascode/SBD, Planar/SBD, Trench/SBD; IGBT/SBD; IGBT/PiN.

Observing Fig. 12, it is important to note that the biggest loss contributors to the total power loss of the SiC transistor technologies is the SiC SBD. The silicon PiN diode exhibits lower conduction losses although it comes with switching losses due to reverse recovery from stored charge. At higher switching frequencies, the performance improvement of SiC SBDs and MOSFETs over PiN diodes/IGBTs will become more apparent. However, at 12kHz, these simulations show that the silicon PiN diode is still very competitive. It can also be seen that the switching losses of the IGBT are affected by the accompanying diode with the IGBT/SBD combination showing better switching performance than the IGBT/PiN combination. This is due to the absence of reverse recovery current in SBDs as shown in Fig. 7.

B. Case 2 – full power acceleration

In this case, the speed profile in the time period between 125 and 145 s of New European Driving Cycle (NEDC) is used. The torque is acquired from the peak performance LUT from the manufacturer. Case 2 represents the vehicle running at its peak performance for acceleration. And in order to achieve the max torque (350 N · m), the peak current (amplitude is 800 A) is demanded from the motor by the traction inverter. Compared to case 1, the power demand on the inverter is significantly higher, hence, the devices operate at significantly higher load current. The simulated power losses (using the experimentally measured conduction and switching energies) is shown in Fig. 15. Fig. 16 shows the vehicle speed, motor torque, stator current and active/reactive power at the stator side in Case 2.

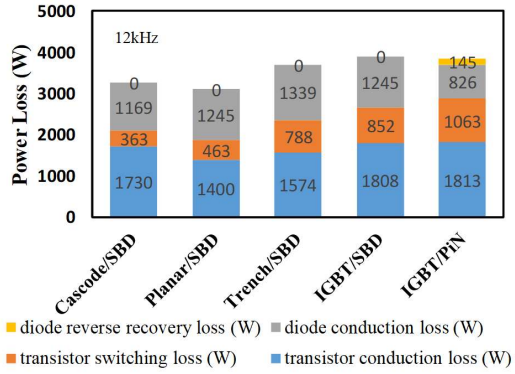

Fig. 15. Average power loss during NEDC cycle 125-145s with peak performance.

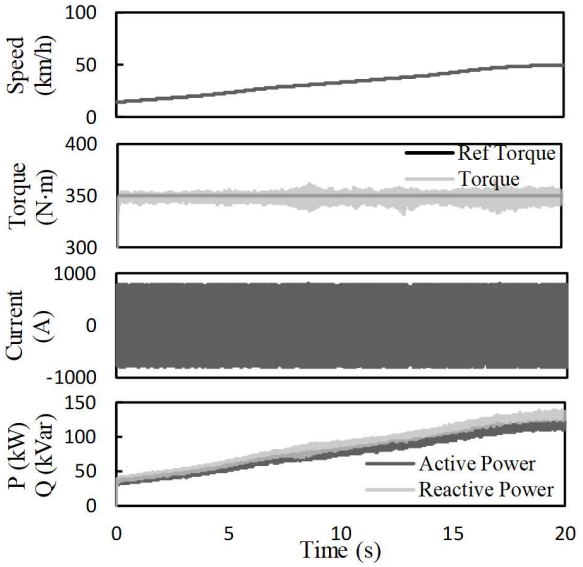

Fig. 16. Operating conditions during NEDC cycle 125-145s with peak performance, from top to bottom are: vehicle speed, motor torque, stator current, electric active and reactive power of the motor.

In terms of power loss shown in Fig. 15, the advantages of SiC devices reduce at higher load currents. Although SiC cascode and planar devices still exhibit superior performance on switching loss, their conduction losses have increased significantly compared to Case 1. The SiC Planar/SBD technology performs the best due to the low conduction loss in the SiC planar MOSFET. As far as switching losses are concerned the SiC Cascode is the best performing technology. The silicon PiN diode, due to its bipolar nature, has better conduction loss performance than the SiC SBD hence, the PiN diode outperforms the SiC SBD in this case.

In this heavy-load case, the cascode device has the best performance with respect to average junction temperature as shown in Fig. 17. The IGBTs show significantly higher junction temperature and swings than the SiC devices. It worth noting that all junction temperature fluctuations show a decreasing trend with the increase of the vehicle speed. This is because at higher speed, the current fundament frequency is higher thus power dissipation cycle is shorter which eventually results in smaller temperature fluctuation.

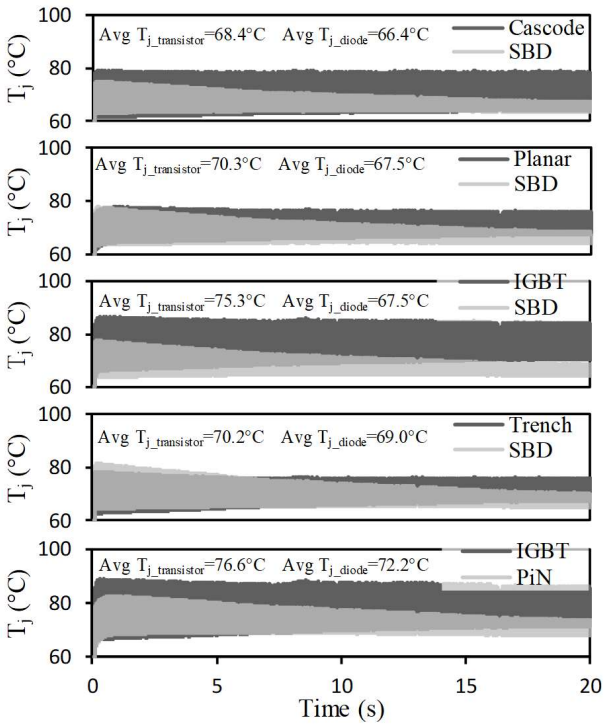

Fig. 17. Junction Temperatures, from top to bottom are: Cascode/SBD; Planar/SBD; Trench/SBD; IGBT/SBD; IGBT/PiN.

It can be observed from Fig. 12 and 15, that the conduction loss of the SiC SBD is a major contribution to the total losses. It is important to mention that this loss can potentially be reduced by using the SiC MOSFETs as a synchronous rectifier during 3rd quadrant operation. This will however add complexity to the controls of the converter.

C. Case 3 – same current density comparison in full power acceleration

The operating condition of this case is identical to Case 2 shown in Fig. 16, i.e. NEDC: 125-145 s. However, in this case, the numbers of devices are selected to target a defined current density of 3.16 A/mm^2 i.e. the total semiconductor area is the same. Here the SiC devices operate at reduced current densities.

Fig. 18 shows that the SiC cascode device exhibits the best performance, followed by the SiC planar MOSFET, the SiC Trench MOSFET and then the IGBTs. Similar to Case 2, the IGBT/PiN diode outperforms the IGBT/SiC SBD due to the high conduction losses of the Schottky diode. The junction temperature plots in Fig. 19 show that the SiC cascode JFETs produce the least junction temperature fluctuation followed by the planar MOSFET and the trench MOSFET. In all three cases, the SiC MOSFETs perform better than the Silicon IGBTs in terms of conduction losses, switching losses and junction temperature fluctuation. However, the impact of the higher EMI due to electromagnetic oscillations and the impact of higher dV/dt on motor insulation windings should be considered [25]. The higher dV/dt coupled with parasitic capacitances in the cables, motors and converters cause higher common mode currents as well as other problems like voltage reflections which have a negative impact on motor insulation [26].

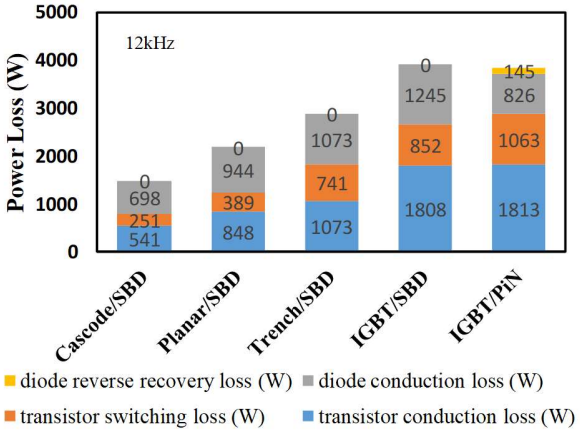

Fig. 18. Average power loss during NEDC cycle 125-145s with peak performance, numbers of devices are chosen to have the same current density.

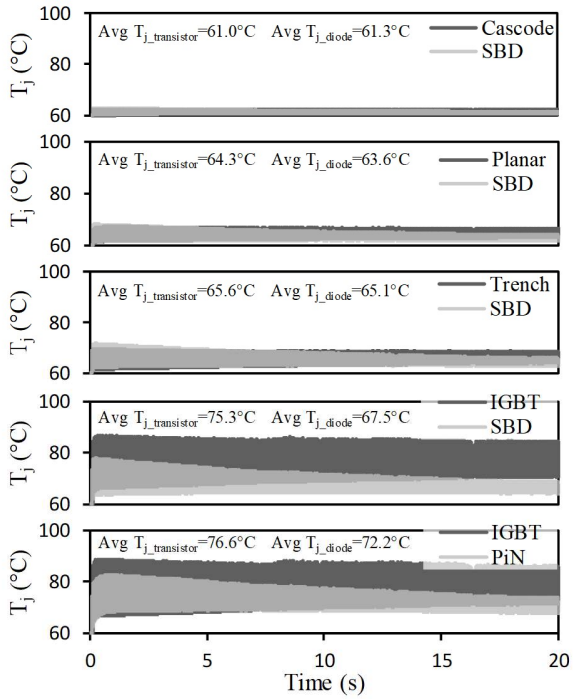

Fig. 19. Junction Temperatures, from top to bottom are: Cascode/SBD; Planar/SBD; Trench/SBD; IGBT/SBD; IGBT/PiN.

D. Case 4 – locked rotor condition

In this case, the critical junction temperature of the devices in the traction converter is investigated. The locked rotor simulation can be seen as a special condition of Case 2 where the vehicle speed is limited at 1km/h. The converter current is at the peak value with very low fundamental frequency which results in the maximum swings to the device junction temperature.

In terms of the power loss shown in Fig. 20, the result is very similar to Case 2. The SiC Planar/SBD technology still performs the best as a whole and SiC Cascode performs best on switching. The silicon PiN diode performs better than SiC SBD on conduction loss due to its bipolar nature.

In this locked rotor case, the cascode device has the best performance with respect to average junction temperature and the Planar device has the smallest swing as shown in Fig. 21. The IGBTs still have higher junction temperature and swings than the SiC devices. This can potentially be an advantage of SiC devices as larger swings tend to result in shorter lifetime of the device [27, 28].

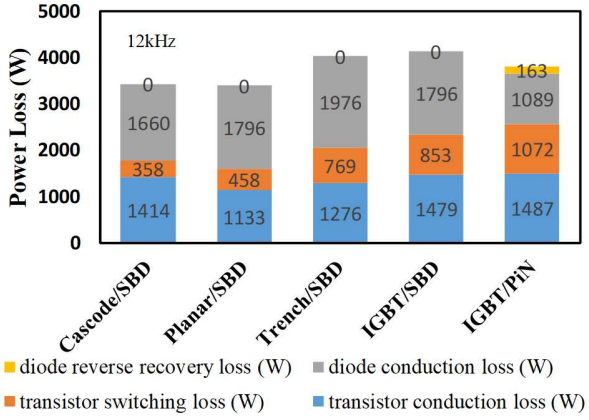

Fig. 20. Average power loss in locked rotor condition.

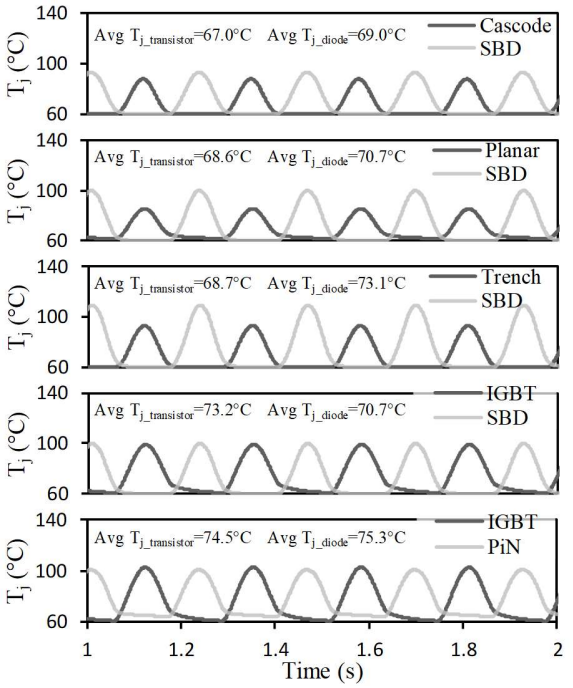

Fig. 21. Junction Temperatures, from top to bottom are: Cascode/SBD; Planar/SBD; Trench/SBD; IGBT/SBD; IGBT/PiN.

V. CONCLUSION

This paper has presented a technical review of the measured and simulated performances of the latest generation SiC power MOSFETs, Cascode JFETs and silicon IGBTs. A 12 kHz EV traction inverter has been simulated (in MATLAB Simulink) using measured device characteristics. Hence, unlike other inverter models where formulas are used with datasheet

parameters, this simulation accounts for the current and temperature dependence of the conduction and switching losses by using experimental static and dynamic measurements. This model therefore represents a more accurate prediction of the EV inverter.

Various driving cycles that subject the traction inverter to different operating conditions (different active/reactive power and fundamental frequencies) have been used to investigate the power loss and junction temperature performances of the different technologies. These cycles include average speed/low torque, acceleration with maximum torque and locked rotor conditions. The main conclusion is that the electrothermal performance of the device technologies depends strongly on the operating point of the converter (speed and torque conditions) as well as the operating current density of the device technologies.

Under low power conditions, the SiC devices outperform the silicon IGBTs with the SiC cascode JFET showing the best performance followed by the SiC planar MOSFET and the SiC Trench MOSFET. The IGBTs with the SiC SBDs outperform the IGBTs with the SiC SBDs due to the superior switching performance of the SBDs. Under high power conditions, during EV acceleration with constant peak torque, the advantages of the SiC devices over the IGBTs reduce since the conduction losses increase significantly. The SiC planar MOSFET marginally outperforms the SiC cascode JFET. The SiC cascode device has relatively higher conduction loss and lower switching loss compared to the SiC planar device. The advantage of the SiC SBD over the PiN diode is not evident under these conditions since the conduction loss of the SBD is higher. However, if switching frequencies are increased in future EVs, SiC SBDs may be the preferable option due to excellent switching performance. Under locked rotor conditions with high torque and low speed, the power devices are subjected to the highest current densities and electrothermal stress. Similar to high power condition, the SiC planar MOSFET marginally outperforms SiC cascode JFET (about 1% less loss). It is worth noting that although SiC Planar has the smallest swing in junction temperature, SiC cascode JFET has the lowest average junction temperature. In terms of diodes under locked rotor condition, the conduction loss of the SiC SBD is around 50% higher than that of the silicon PiN diode. In spite of the improved switching performance of Schottky diodes, PiN diodes have better conduction performance especially at higher junction temperatures. Overall, with regard to power loss and thermal management, SiC cascode JFET shows great potential for EV traction inverters in addition to avoiding the gate oxide reliability issues with SiC MOSFETs.

Inverter simulations were also performed for all technologies operating at the same current density assuming equal chip area. This will have negative cost implications (for SiC devices) but will be good for reliability and thermal management since the devices will operate at reduced current density and junction temperature. Results show that the SiC cascode device performs the best in terms of losses and junction temperatures, followed by the SiC planar MOSFET and the SiC Trench MOSFET.

References

[1] K. Hamada, M. Nagao, M. Ajioka, and F. Kawai, "SiC—Emerging Power Device Technology for Next-Generation Electrically Powered Environmentally Friendly Vehicles," *IEEE Transactions on Electron Devices,* vol. 62, no. 2, pp. 278-285, 2015, doi: 10.1109/TED.2014.2359240.

[2] H. Zhang, L. M. Tolbert, and B. Ozpineci, "Impact of SiC Devices on Hybrid Electric and Plug-In Hybrid Electric Vehicles," *IEEE Transactions on Industry Applications,* vol. 47, no. 2, pp. 912-921, 2011, doi: 10.1109/TIA.2010.2102734.

[3] S. K. Singh, F. Guédon, P. J. Garsed, and R. A. McMahon, "Half-bridge SiC inverter for hybrid electric vehicles: Design, development and testing at higher operating temperature," in *6th IET International Conference on Power Electronics, Machines and Drives (PEMD 2012)*, 27-29 March 2012 2012, pp. 1-6, doi: 10.1049/cp.2012.0312.

[4] F. Xu *et al.*, "Development of a SiC JFET-Based Six-Pack Power Module for a Fully Integrated Inverter," *IEEE Transactions on Power Electronics,* vol. 28, no. 3, pp. 1464-1478, 2013, doi: 10.1109/TPEL.2012.2205946.

[5] M. Su, C. Chen, S. Sharma, and J. Kikuchi, "Performance and cost considerations for SiC-based HEV traction inverter systems," in *2015 IEEE 3rd Workshop on Wide Bandgap Power Devices and Applications (WiPDA)*, 2-4 Nov. 2015 2015, pp. 347-350, doi: 10.1109/WiPDA.2015.7369032.

[6] M. Nakanishi *et al.*, "Automotive Traction Inverter Utilizing SiC Power Module," in *PCIM Europe 2018; International Exhibition and Conference for Power Electronics, Intelligent Motion, Renewable Energy and Energy Management*, 5-7 June 2018 2018, pp. 1-6.

[7] C. Zhang, S. Srdic, S. Lukic, Y. Kang, E. Choi, and E. Tafti, "A SiC-Based 100 kW High-Power-Density (34 kW/L) Electric Vehicle Traction Inverter," in *2018 IEEE Energy Conversion Congress and Exposition (ECCE)*, 23-27 Sept. 2018 2018, pp. 3880-3885, doi: 10.1109/ECCE.2018.8558373.

[8] E. Gurpinar and B. Ozpineci, "Loss Analysis and Mapping of a SiC MOSFET Based Segmented Two-Level Three-Phase Inverter for EV Traction Systems," in *2018 IEEE Transportation Electrification Conference and Expo (ITEC)*, 13-15 June 2018 2018, pp. 1046-1053, doi: 10.1109/ITEC.2018.8450188.

[9] F. Shang, A. P. Arribas, and M. Krishnamurthy, "A comprehensive evaluation of SiC devices in traction applications," in *2014 IEEE Transportation Electrification Conference and Expo (ITEC)*, 15-18 June 2014 2014, pp. 1-5, doi: 10.1109/ITEC.2014.6861777.

[10] D. Oustad, M. Ameziani, D. Lhotellier, S. Lefebvre, and M. Petit, "Estimation of the Losses in Si and SiC Power Modules for Automotive Applications," in *PCIM Europe 2017; International Exhibition and Conference for Power Electronics, Intelligent Motion, Renewable Energy and Energy Management*, 16-18 May 2017 2017, pp. 1-8.

[11] W. Chou, A. Kempitiya, and O. Vodyakho, "Reduction of Power Losses of SiC MOSFET Based Power Modules in Automotive Traction Inverter Applications," in *2018 IEEE Transportation Electrification Conference and Expo (ITEC)*, 13-15 June 2018 2018, pp. 1035-1038, doi: 10.1109/ITEC.2018.8450130.

[12] A. Kempitiya and W. Chou, "Electro-thermal simulation for high power IGBTs for automotive applications," in *2016 22nd International Workshop on Thermal Investigations of ICs and Systems (THERMINIC)*, 21-23 Sept. 2016 2016, pp. 58-62, doi: 10.1109/THERMINIC.2016.7748648.

[13] A. P. Pai, T. Reiter, and M. Maerz, "Efficiency Investigation of Full-SiC versus Si-based Automotive Inverter Power Modules at Equal Commutation Speed," in *PCIM Europe 2018; International Exhibition and Conference for Power Electronics, Intelligent Motion, Renewable Energy and Energy Management*, 5-7 June 2018 2018, pp. 1-8.

[14] J. Zhu, H. Kim, H. Chen, R. Erickson, and D. Maksimović, "High efficiency SiC traction inverter for electric vehicle applications," in *2018 IEEE Applied Power Electronics Conference and Exposition (APEC)*, 4-8 March 2018 2018, pp. 1428-1433, doi: 10.1109/APEC.2018.8341204.

[15] X. Ding *et al.*, "Analytical and Experimental Evaluation of SiC-Inverter Nonlinearities for Traction Drives Used in Electric Vehicles," *IEEE Transactions on Vehicular Technology,* vol. 67, no. 1, pp. 146-159, 2018, doi: 10.1109/TVT.2017.2765670.

[16] K. Puschkarsky, H. Reisinger, T. Aichinger, W. Gustin, and T. Grasser, "Understanding BTI in SiC MOSFETs and Its Impact on Circuit Operation," *IEEE Transactions on Device and Materials Reliability,* vol. 18, no. 2, pp. 144-153, 2018, doi: 10.1109/TDMR.2018.2813063.

[17] J. A. O. González and O. Alatise, "A Novel Non-Intrusive Technique for BTI Characterization in SiC mosfets," *IEEE Transactions on Power Electronics,* vol. 34, no. 6, pp. 5737-5747, 2019, doi: 10.1109/TPEL.2018.2870067.

[18] K. Puschkarsky, T. Grasser, T. Aichinger, W. Gustin, and H. Reisinger, "Understanding and modeling transient threshold voltage instabilities in SiC MOSFETs," in *2018 IEEE International Reliability Physics Symposium (IRPS)*, 11-15 March 2018 2018, pp. 3B.5-1-3B.5-10, doi: 10.1109/IRPS.2018.8353560.

[19] R. Xie, Y. Shi, and H. Li, "Study of 1200 V SiC JFET cascode device," in *2017 IEEE 5th Workshop on Wide Bandgap Power Devices and Applications (WiPDA)*, 30 Oct.-1 Nov. 2017 2017, pp. 316-320, doi: 10.1109/WiPDA.2017.8170566.

[20] J. Bendel, "Cascode Configuration Eases Challenges of Applying SiC JFETs," ed: United Silicon Carbide, 2016.

[21] J. Pyrhonen, V. Hrabovcova, and R. S. Semken, *Electrical machine drives control: An introduction*. John Wiley & Sons, 2016.

[22] L. Harnefors and H. Nee, "Model-based current control of AC machines using the internal model control method," *IEEE Transactions on Industry Applications,* vol. 34, no. 1, pp. 133-141, 1998, doi: 10.1109/28.658735.

[23] L. Wang, *Modeling and control of sustainable power systems: Towards smarter and greener electric grids*. Springer, 2011.

[24] J. Pou, D. Osorno, J. Zaragoza, C. Jaen, and S. Ceballos, "Power losses calculation methodology to evaluate inverter efficiency in electrical vehicles," in *2011 7th International Conference-Workshop Compatibility and Power Electronics (CPE)*, 1-3 June 2011 2011, pp. 404-409, doi: 10.1109/CPE.2011.5942269.

[25] A. K. Morya *et al.*, "Wide Bandgap Devices in AC Electric Drives: Opportunities and Challenges," *IEEE Transactions on Transportation Electrification,* vol. 5, no. 1, pp. 3-20, 2019, doi: 10.1109/TTE.2019.2892807.

[26] O. Alatise, N. Parker-Allotey, D. Hamilton, and P. Mawby, "The Impact of Parasitic Inductance on the Performance of Silicon–Carbide Schottky Barrier Diodes," *IEEE Transactions on Power Electronics,* vol. 27, no. 8, pp. 3826-3833, 2012, doi: 10.1109/TPEL.2012.2183390.

[27] R. Bayerer, T. Herrmann, T. Licht, J. Lutz, and M. Feller, *Model for Power Cycling lifetime of IGBT Modules - various factors influencing lifetime*. 2008, pp. 1-6.

[28] W. Lai, M. Chen, L. Ran, O. Alatise, S. Xu, and P. Mawby, "Low ΔT_j Stress Cycle Effect in IGBT Power Module Die-Attach Lifetime Modeling," *IEEE Transactions on Power Electronics,* vol. 31, no. 9, pp. 6575-6585, 2016, doi: 10.1109/TPEL.2015.2501540.